Available online at www.sciencedirect.com

ScienceDirect

Ceramics International 40 (2014) 11089–11097

CERAMICS INTERNATIONAL

www.elsevier.com/locate/ceramint

Graphene–titania films by supersonic kinetic spraying for enhanced performance of dye-sensitized solar cells

Do-Yeon Kim[1,a], Bhavana N. Joshi[1,a], Jung-Jae Park[a], Jong-Gun Lee[a], You-Hong Cha[a], Tae-Yeon Seong[b], Suk In Noh[b], Hyo-Jin Ahn[c], Salem S. Al-Deyabe[d], Sam S. Yoon[a,*]

[a]School of Mechanical Engineering, Korea University, Seoul, Republic of Korea
[b]Department of Materials Science and Engineering, Korea University, Seoul, Republic of Korea
[c]Department of Materials Science and Engineering, Seoul National University of Science and Technology, Seoul, Republic of Korea
[d]Petrochemical Research Chair, Department of Chemistry, College of Science, King Saud University, Riyadh 11451, Saudi Arabia

Received 19 February 2014; received in revised form 24 March 2014; accepted 24 March 2014
Available online 29 March 2014

Abstract

Graphene–titania films were fabricated by supersonic kinetic spray, known as aerosol deposition. Graphene concentration was varied to fabricate 0.1, 0.3, 0.5, 0.7, and 1.0 wt% G–TiO_2 films for dye-sensitized solar cell (DSSC) application and to investigate the effect of graphene concentration on their energy conversion efficiency. The G–TiO_2 films were characterized and analyzed based on results from SEM, XRD, XPS, TEM, and the current–voltage curve. The optimal concentration was 0.3 wt%, which decreased the recombination rate, favoring the formation of photogenerated electron–hole pairs. As a result, the conversion efficiency was 5.02% while that of the pure TiO_2 was 3.14%. A clear trend per various concentrations was observed. At higher concentrations than 0.3 wt%, the conversion efficiency decreased owing to higher absorption of light by graphene present on the surface, thus reducing the generation of electron–hole pairs.

Keywords: Graphene-titania; Dye-sensitized solar cell; Aerosol deposition; Supersonic kinetic spraying

1. Introduction

Photosynthesis is one of the natural processes that occurs in plants, and dye-sensitized solar cells (DSSCs), originally developed by O'Regan and Gratzel [1]. DSSCs have become a promising alternative to conventional silicon solar cells owing to its low cost and high efficiency. Titania or TiO_2 is a frequently used photocatalytic material in DSSCs; it has many other applications as well, such as for self-cleaning products [2], water and air purification [3], destruction of cancer cells [4] and viruses, and medical applications [5]. DSSCs consist of a transparent conducting oxide (TCO) electrode, dye (generally a ruthenium dye), and a mesoporous layer of a wide-band-gap semiconductor (usually TiO_2) [6]. Many researchers have attempted to increase the efficiency of DSSCs by tailoring the surface area of the TiO_2 layer by creating mesoporosity, as well as by varying the dopants and using high-performance dyes. Doping TiO_2 with various materials such as nitrogen [7], sulfur [8], niobium [9], and carbon [10] have already been reported to improve the optical absorption in visible light for enhancing the efficiency of DSSCs.

Graphene is well known for its high conductivity, mechanical strength, energy gap tenability, and high elasticity. These unique properties are useful in the hydrothermal field, and in devices such as transparent conducting oxides (TCOs) and lithium ion batteries [11,12]. Furthermore, graphene-based materials are known to act as antibacterial agents [13]. As mentioned earlier, the addition of a metallic material such as carbon, graphene, or carbon nanotubes (CNTs) in the TiO_2 layer is expected to enhance the photocatalytic activity of TiO_2 because of faster electron transfer that also hinders the undesirable recombination of excited electrons [14–17]. Enhanced photocatalytic ability by combining TiO_2 with reduced graphene oxide (rGO) for DSSCs

*Corresponding author.
E-mail address: skyoon@korea.ac.kr (S.S. Yoon).
[1]Equal contribution.

http://dx.doi.org/10.1016/j.ceramint.2014.03.131
0272-8842/

has already been reported [18–20]. Moreover, it has been reported that multiwalled carbon nanotubes (MWCNTs), single-walled carbon nanotubes (SWCNTs), and graphene have highly beneficial effects on the photocatalytic activity, which is used to promote antibacterial activity [21], degradation of phenol [14,22], and the reaction of methylene blue (MB) [23,24].

The aerosol deposition (AD) method used in this study is a type of gas-deposition method, in which a high-velocity gas jet is used to accelerate feedstock powder to form a colloidal aerosol flow. These accelerated powder particles collide with the substrate at high velocity and form a dense film at room temperature (RT). AD is a low-cost process; moreover, there is no phase transition during deposition. The AD-coating mechanism is related to the kinetic and fracture energy of the particle. Akedo [25] reported the importance of the initial powder size. They demonstrated that an initial particle size of less than 50 nm means particles are lightweight, and thus pressing them into a compact form is difficult because of their low kinetic energy. Similarly, Ryu et al. [26] reported that TiO_2 powder tens of nanometers in size could not be deposited because of the low kinetic energy. Tang et al. [18] reported that graphene sheets–TiO_2 composite films on indium tin oxide coated glass were prepared by electrophoretic deposition, and the conversion efficiency was 1.68% while that of the pure TiO_2 without graphene sheets was 0.32%.

We herein describe a new and simple synthesis method to distribute graphene flakes in TiO_2 powder. This new powder synthesis method is based on the initial steps used in the sol–gel [27] process, including the use of a doctor blade [28], and spin coating [29]. The graphene–TiO_2 solution prepared here is advantageous as graphene is easily distributed with TiO_2 powder. TiO_2 powder mixed with a polymer increases the size of the particles to a few micrometers. Thus, the poly(vinyl alcohol) (PVA) polymer combined with graphene and TiO_2 acts as a glue in this method. In our previous study [30], we reported the deposition of TiO_2 films on a glass substrate by AD without the use of a carrier solvent. However, as mentioned earlier, the AD method could not produce TiO_2 films using nanosized particles such as P25 TiO_2 powder [25,26]. Hence, we introduce here a unique method for use with the AD coating. We prepared micron-sized aggregated G–TiO_2 powder to make films by the AD method. The G–TiO_2 composite powders were prepared by employing graphene and P25 (80% anatase and 20% rutile) as the starting materials at room temperature. Various graphene concentrations were incorporated with the TiO_2 films, which were then used as working electrodes in DSSCs.

2. Experimental setup

2.1. G–TiO_2 composite

The TiO_2 powder (P25, $d_{50} \approx 25$ nm) used in the study was purchased from Degussa (Birmingham, AL, USA) and was a mixture of an 80% anatase phase and a 20% rutile phase. A poly(vinyl alcohol) polymer (Sigma-Aldrich Corp., USA) was used for making micron-sized particles of P25 powder. Graphene powder (Grade M25, average diameter of ~25 μm, less than 1.0 wt% oxygen) was provided by XG Sciences, Inc. (USA).

The fabrication process of the G–TiO_2 powder is schematically illustrated in Fig. 1. First, P25 (200 g) and de-ionized (DI) water (500 mL) were stirred together and then 0.1–1.0 wt% of graphene powder was added to make the G–TiO_2 colloidal suspension, which was continuously stirred for 24 h. Then, 5 g of PVA (MW 22,000) was dissolved in water by stirring it at room temperature. A G–TiO_2 paste was then prepared by the drop-wise addition of the PVA solution, which was then annealed at 300 °C for 30 min. A pulverization process was used to prevent agglomeration of the G–TiO_2 composite powder. Finally, micron-size G–TiO_2 composite powder was prepared by a ball-milling process carried out for 1 day.

2.2. Aerosol deposition

The G–TiO_2 films were fabricated by the AD method reported in our previous work [31]. The experimental setup of AD consisted of a gas tank, fluidized bed powder feeder, nozzle, vacuum chamber, two-dimensional (2D) x–y stage, booster pump, and vacuum pump, as shown in Fig. 2(a). Aggregated G–TiO_2 composite powder was pre-mixed with

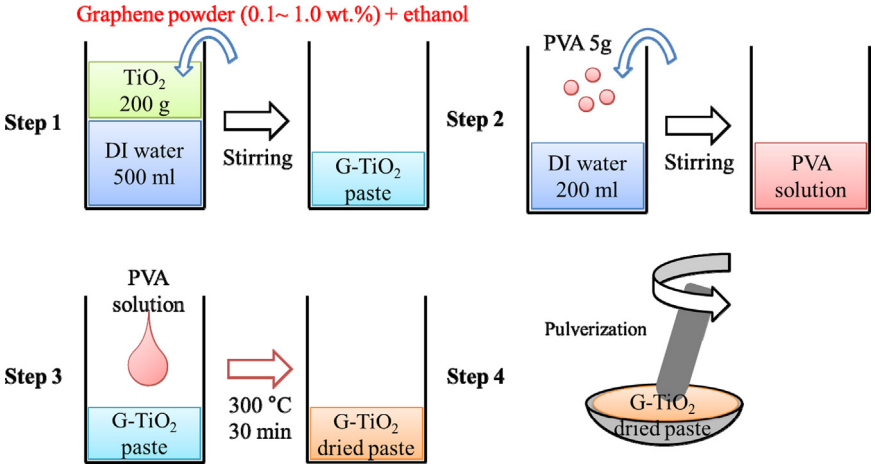

Fig. 1. Synthesis process for G–TiO_2 powder.

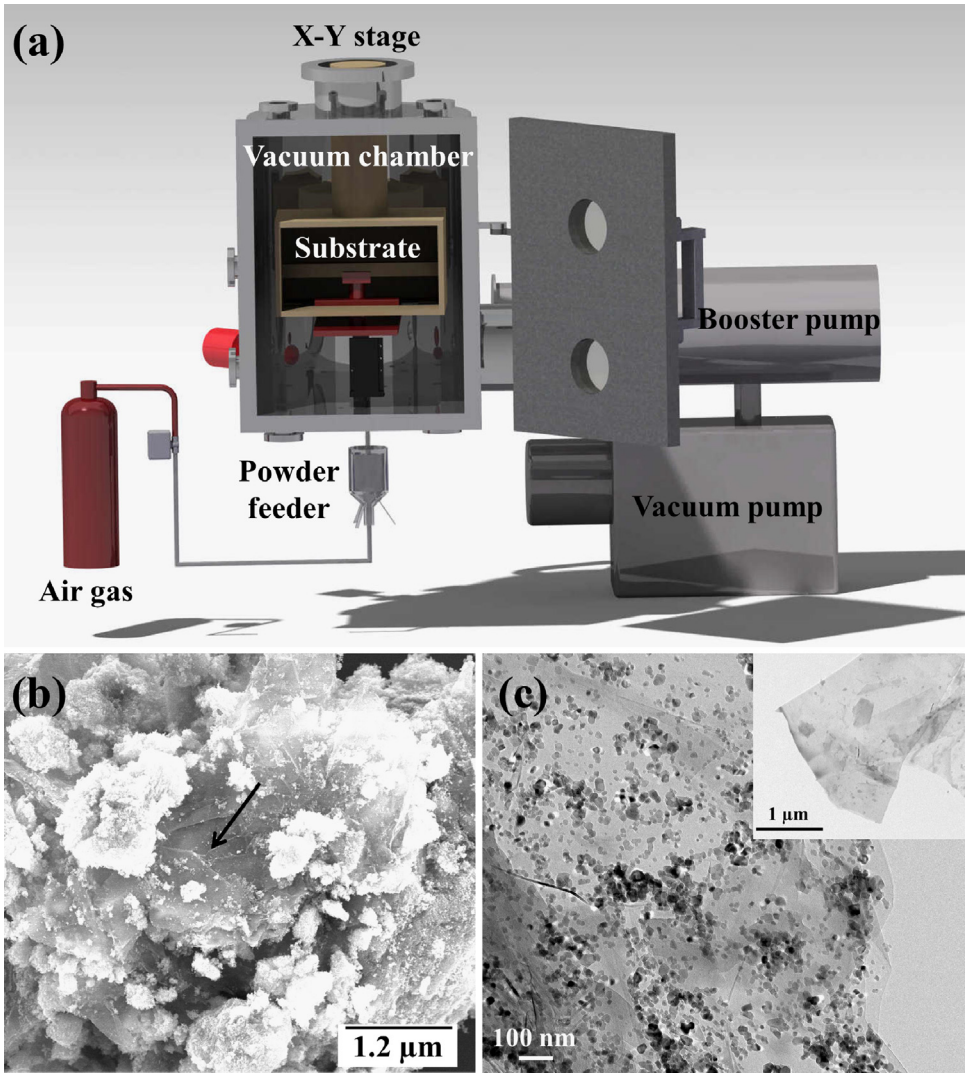

Fig. 2. (a) Schematic of the aerosol deposition system, (b) SEM and (C) TEM images of G–TiO_2 powder.

dry air in the fluidized bed, fed into the nozzle, and accelerated at a supersonic speed. The particle-laden air was injected into the deposition chamber evacuated by vacuum and booster pumps. The deposition chamber was evacuated P_{amb} = 0.35–5.6 Torr to minimize TiO_2 particle deceleration before impact. The experimental conditions used for film deposition are summarized in Table 1.

All G–TiO_2 films were deposited at room temperature onto fluorine-doped tin oxide (FTO)-coated glasses provided by Pilkington, Tokyo, Japan (8 Ω/cm^2). The FTO substrates were cleaned in an ultrasonic acetone bath for 10 min before use. The as-deposited films were annealed at 500 °C for 0.5 h to improve the adhesion of the G–TiO_2 films.

2.3. Cell fabrication

The G–TiO_2 films of various graphene concentrations were sensitized with 0.5 mM of cis-dithiocyanato-bis(4,4′-dicarboxy-2, 2′-bypyridine) ruthenium(II) [$Ru(dcbpy)_2(NCS)_2$] dye (from Solaronix) for 24 h. An electrolyte was prepared with 0.5 M of LiI (Sigma-Aldrich), 0.05 M of I_2 (Merck), 0.5 M of 4-tert-butylpyridine (Sigma-Aldrich), and 0.3 M of DMPII (Solaronix) in a 3-MPN solution (Sigma-Aldrich) [32]. For the counter electrode, a Pt-coated FTO glass was prepared by drop-wise addition of 0.5–1.0 mL of a Pt solution. The Pt solution was prepared by dissolving H_2PtCl_6 (Sigma-Aldrich) in 2-propanol (Sigma-Aldrich) under heat treatment at 450 °C for 30 min. Then, DSSCs were assembled as typical sandwich-type cells. The thickness and active area of the cells were approximately 7.5 μm and 0.5 × 0.5 cm^2, respectively. Cell measurements were carried out using a 150-W xenon lamp (LAB50) at AM 1.5 G irradiation conditions.

2.4. Characterizations

The surface microstructure of the deposited G–TiO_2 powder and films were characterized with high-resolution scanning electron microscopy (HRSEM, XL30SFEG Phillips Co., Holland) at 10 kV and transmission electron microscopy (TEM, EM420, Philips Electron Optics, Eidhoven, Holland).

X-ray diffraction (XRD, D/MAX-2500, Rigaku Japan) was used to study the structural properties of the films. X-ray photoelectron spectroscopy (XPS, PHI5600, Physical Electronics) was also carried out to analyze the elemental compositions and assign the carbon peaks. The absorption spectra were obtained using a UV–vis spectrophotometer (OPTIZEN POP, Mecasys Co. LTD, Korea) at $190 \leq \lambda \leq 1100$ nm. The photoluminescence (PL) spectra were obtained by using a Hitachi F-7000 FL spectrophotometer.

Table 1
Experimental conditions.

Pressure in deposition chamber [Torr]	0.35–5.6
Propellant gas	Air
Nozzle exit area [mm^2]	10×35
Stand-off distance [mm]	5
Gas temperature	RT (20 °C)
Consumption of propellant gas [L/min]	7
Stage traverse speed [mm/s]	0.72
Number of passes	1

3. Results and discussion

Fig. 2(b) is an SEM image of the 0.1 wt% G–TiO_2 powder prepared by AD. The arrow shows the graphene flakes, and aggregated TiO_2 particles several micrometers in size are attached to the graphene flake. The nanosized TiO_2 particles were agglomerated using the PVA polymer. The TEM image of the 0.1 wt% G–TiO_2 powder is presented in Fig. 2(c), which clearly reveals that the TiO_2 particles are evenly distributed around the graphene flakes. The inset of the TEM image shows the original graphene flakes used in this study.

Fig. 3(a–f) are the SEM images of the top and cross-sectional views of the AD-deposited G–TiO_2 films. It seems that the average thickness of most of the films was approximately ~7.5 μm, except for the 0.3 wt% case, as in Fig. 3c. The film roughness varied quite significantly depending on the amount of G–TiO_2 powder. As mentioned, the graphene size extended up to ~25 μm. Thus, a region in which relatively greater amount of G–TiO_2 powder was deposited produced a thicker film locally, as opposed to the region of lesser amount of G–TiO_2. As observed in the figure, the G–TiO_2 films were

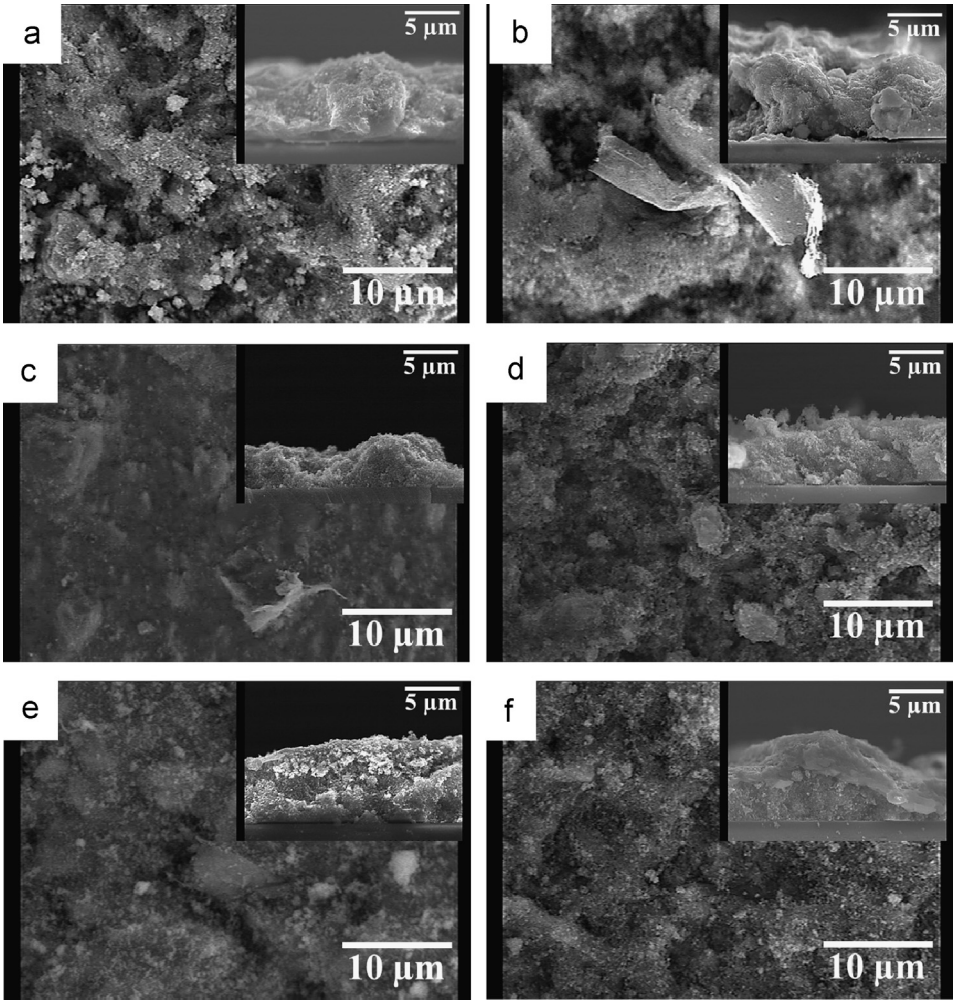

Fig. 3. The top-view and cross-sectional SEM images (in inset) of the TiO_2 film on FTO glass, (a) pure, (b) 0.1 wt%, (c) 0.3 wt%, (d) 0.5 wt%, (e) 0.7 wt%, and (f) 1.0 wt%.

pore-free and dense because of the collisions of accelerated TiO_2 particles on the substrate and the use of PVA. The PVA caused the agglomeration of the particles, thus increasing the particle size; it also acted as a glue, binding the graphene and TiO_2 particles. Although the collision of the accelerated G–TiO_2 particles with the substrate leads to strong adhesion, PVA also plays an important role in improving the adhesion between the film and substrate.

Fig. 4 presents the XRD results for the P25 TiO_2 powder, the pure TiO_2, and the G–TiO_2 films deposited by the AD method. The AD method used here is known for maintaining the phases of the raw powder, which is confirmed from the XRD patterns showing anatase and rutile phases. The peaks near 25.3°, 37.8°, 48.0°, 53.9°, 55.1°, 62.7°, and 68.7° were attributed to the (101), (004), (200), (105), (211), (204), and (220) crystal planes, respectively, of the anatase phase (JCPDS 21-1272), whereas the peaks near 27.4°, 36.0°, and 38.6° were indexed to the (110), (100), and (111) crystal planes, respectively, of the rutile phase (JCPDS 21-1276). The crystallite sizes of the films shown in Table 2 were determined by Scherrer's equation, $\tau = K\lambda/(\beta \cos\theta)$, where τ is the mean crystalline size, λ the wavelength, β the full width at half maximum (FWHM) of the diffraction peak, θ the peak position, and K is Scherrer's constant [33].

The crystallite size of the anatase (101) phase of the P25 TiO_2 powder was 24.3 nm, which is close to the actual size of 25 nm. The crystallite size of the anatase and rutile phases of the pure TiO_2 films decreased to 20.2 and 24.4 nm, respectively. These values decreased further to 16.7 and 23.1 nm, respectively, for the 1.0 wt% G–TiO_2 film. This reduction in crystallite size of the films is due to AD, where high-velocity particles directly collide with the substrate, resulting in fragmentation of the impacting powder. A similar reduction of crystallite size of aerosol-deposited films was reported in our previous work [30,31,34]. The characteristic (002) peak of graphene at 25.7° is difficult to identify in all the XRD patterns of the G–TiO_2 films, which may be because the graphene peak is weak and overlaps with the (101) peak of anatase TiO_2 (25.3°) [35].

The photocurrent density–voltage curves of the pure TiO_2 and 0.1, 0.3, 0.5, 0.7, and 1.0 wt% G–TiO_2 shown in Fig. 5 clearly indicate that the G–TiO_2 films have higher photocurrent density than the pure TiO_2. The open-circuit voltage (V_{oc}), short-circuit current density (J_{sc}), fill factor (FF), and efficiency (η) are presented in Table 3. The pure TiO_2 film has a conversion efficiency of 3.14%. Although the G–TiO_2 films have higher efficiency than the pure TiO_2 film, the 0.3 wt% G–TiO_2 film showed the highest conversion efficiency of 5.02%. J_{sc} initially increased with increasing graphene concentration up to 0.3 wt% (J_{sc} = 10.93 mA/cm^2) and then decreased to 8.67 mA/cm^2 at 1.0 wt%. The initial increase and later decrease in J_{sc} can be explained by the increased conductivity of TiO_2 due to graphene inclusion [18]. The gradual increase in the amount of graphene increased the

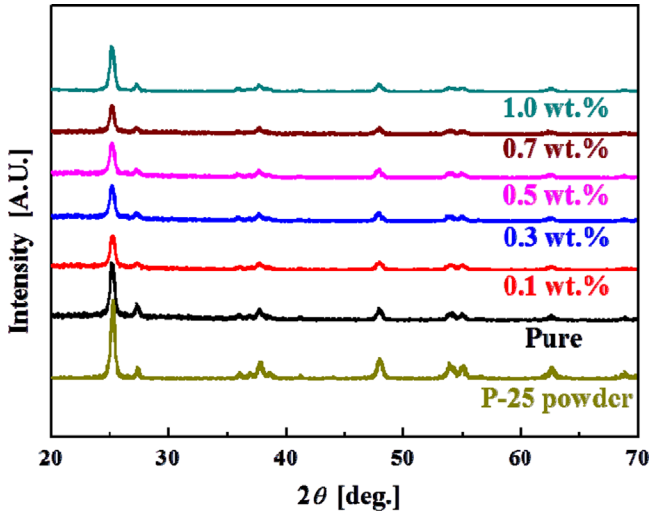

Fig. 4. XRD patterns of P-25 powder, pure, 0.1, 0.3, 0.5, 0.7, and 1.0 wt% G–TiO_2 film.

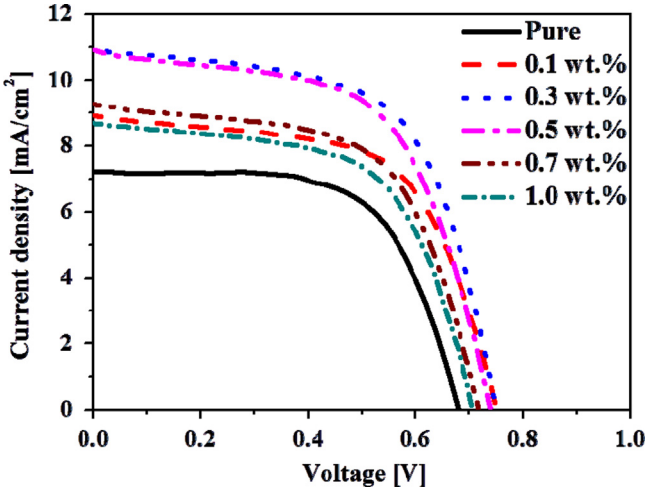

Fig. 5. Photocurrent–voltage data of DSSCs prepared with different graphene concentration (pure, 0.1, 0.3, 0.5, 0.7, and 1.0 wt%) under one sun intensity.

Table 2
Crystallite size of TiO_2 and G-TiO_2 films.

TiO_2 lattice	Crystallite size [nm]		
	Powder	Pure film	1.0 wt% G-TiO2 film
Anatase (101)	24.3	20.2	16.7
Rutile (110)	34.2	24.4	23.1

Table 3
Parameters for DSSCs based on different electrodes.

Sample [wt%]	V_{oc} [V]	J_{sc} [mA/cm^2]	Fill factor [%]	Efficiency [%]
Pure	0.68	7.20	64.26	3.14
0.1	0.75	8.92	60.95	4.08
0.3	0.75	10.93	61.26	5.02
0.5	0.74	10.90	59.12	4.77
0.7	0.72	9.27	60.14	4.00
1.0	0.69	8.67	60.47	3.62

number of photogenerated electrons, making TiO_2 conductive, and thus the electrons easily move through the graphene. As a result, the recombination rate was reduced. Hence, the DSSC efficiency was increased after including graphene in TiO_2 up to 0.3 wt%. However, further increase in the amount of graphene showed lower efficiency. This lower efficiency was primarily due to the strong absorption of light by graphene when the concentration was increased, which reduced light absorption on the TiO_2 surface and therefore decreased the number of photoexcited electrons. The secondary reason for the lower efficiency was the poor crystallinity of G–TiO_2 films. As mentioned earlier, the crystal size of the 1.0 wt% film was lower than that of the pure film. Because of the reduced crystal size at higher graphene concentration, the absorption capacity of the 0.3 wt% film was decreased. On the other hand, V_{oc} and *FF* remained in the range 0.68–0.75 V and 59.12–63.26%, respectively.

To understand the effect of 0.3 wt% graphene with TiO_2, an XPS study was carried out. The Ti_{2p} peaks of pristine TiO_2 and the 0.3 wt% G-TiO_2 films are shown in Fig. 6(a) and (b) respectively. For the pristine case in Fig. 6(a), the two peaks centered at 458.2 and 463.8 eV, which are assigned to $Ti_{2p3/2}$ and $Ti_{2p1/2}$. These peaks reveal that the binding energy difference (or slitting) between $Ti_{2p3/2}$ and $Ti_{2p1/2}$ is approximately 5.6 eV, which is a strong evidence of the presence of Ti^{4+} state [21]. For the 0.3 wt% case in Fig. 6(b), a slight shift in the $Ti_{2p3/2}$ peak from 458.2 to 457.8 eV had occurred. Furthermore, the deconvolution of the Ti_{2p} peak shows two subordinate peaks centered at 457.8 and 458.2 eV which belong to the Ti^{3+} and Ti^{4+} states, respectively [36–38]. The Ti^{3+} state was newly produced in the 0.3 wt% case and was not present in the pristine case. This new state of Ti^{3+} species was originated from the carboxyl groups of graphene linking with titanium via chelation. These carboxyl groups reduced valence of titanium by replacing oxygen from TiO_2, giving rise to the Ti^{3+} state. However, when the graphene content was increased from 0.3 to 1.0 wt%, the binding energy peak of $Ti_{2p3/2}$ is shifted back to 458.2 eV (blue-shift). This blue-shift was caused by the presence of highly electronegative oxygen, which in general attracts electrons from Ti. This oxygen is expected to accumulate during the open-air annealing process carried out at 500 °C for 30 min.

The C1s XPS spectrum of the pristine TiO_2 and 0.3 wt% G–TiO_2 is shown in Fig. 7(a) and (b), respectively. For the pristine case, the broad peak at 284.5 eV is attributed to the C–C bond originating from the sp^2 carbon atoms of graphene

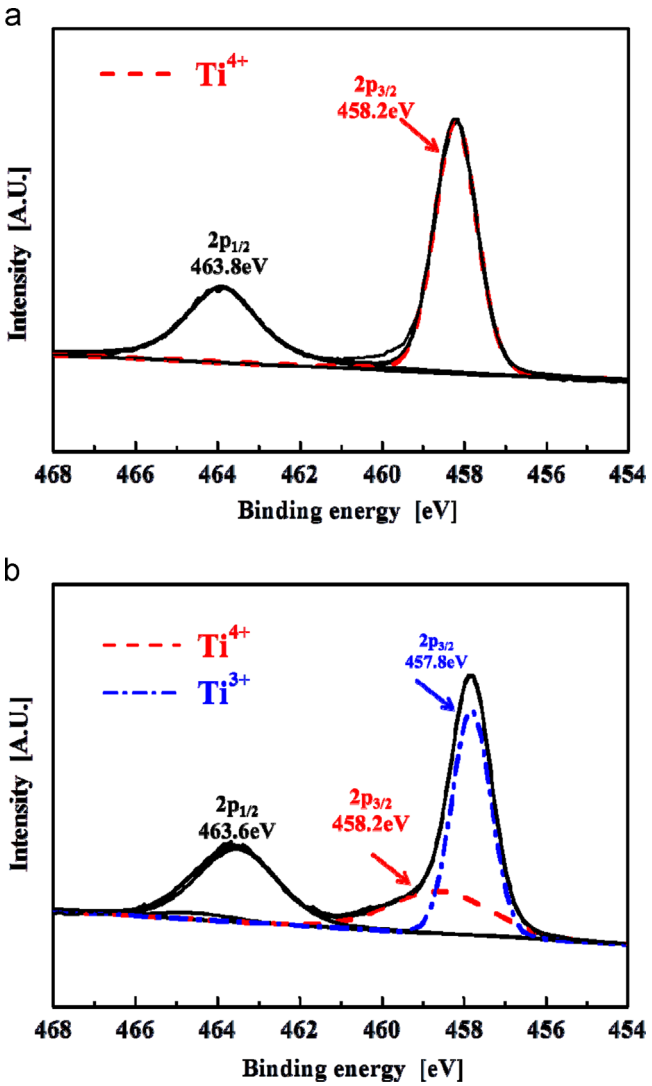

Fig. 6. Deconvoluted XPS spectra of Ti_{2p} peak showing Ti^{3+} and Ti^{4+} states of (a) pristine and (b) 0.3 wt%.

while the weak shoulder peak at 288.26 eV belongs to the C=O bond. The deconvolution of the broad C–C bond peak yields one shoulder peak located at 286 eV originating from the C–O functional groups [21,39]. For the 0.3 wt% case, the C–C, C–O, and C=O bonds are observed at 284.4, 285.6, and 288.2 eV, respectively, as in Fig. 7(b). The Ti–C carbonaceous bonds also appeared. This Ti–C bond is expected to form between TiO_2 and the graphene flakes during the annealing

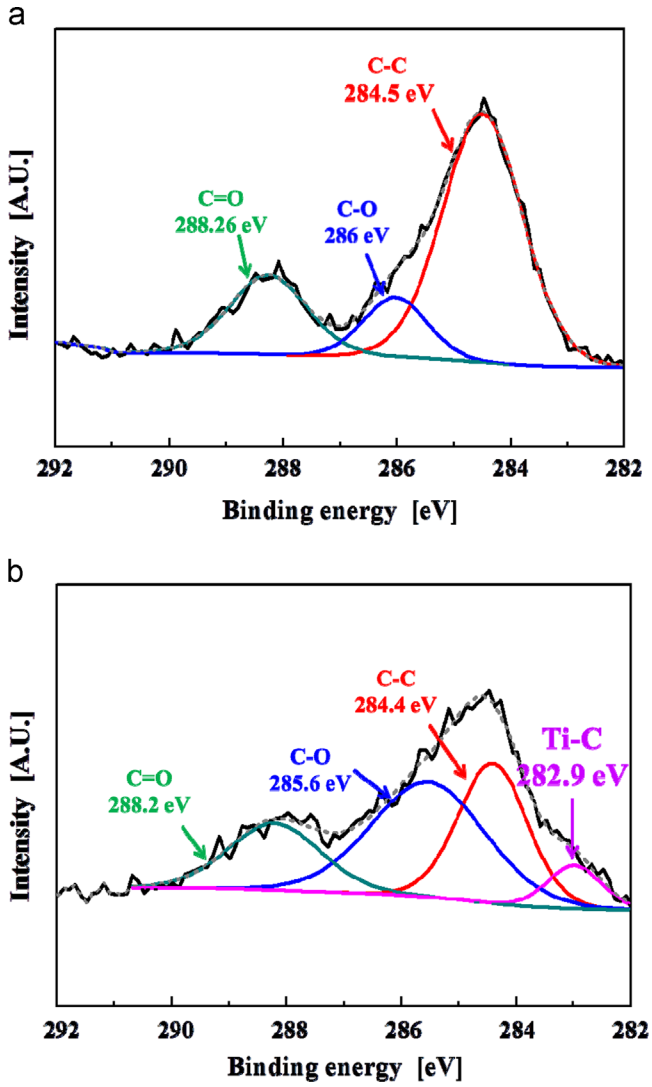

Fig. 7. Peak deconvolution of the C1s core level (a) pristine and (b) 0.3 wt%.

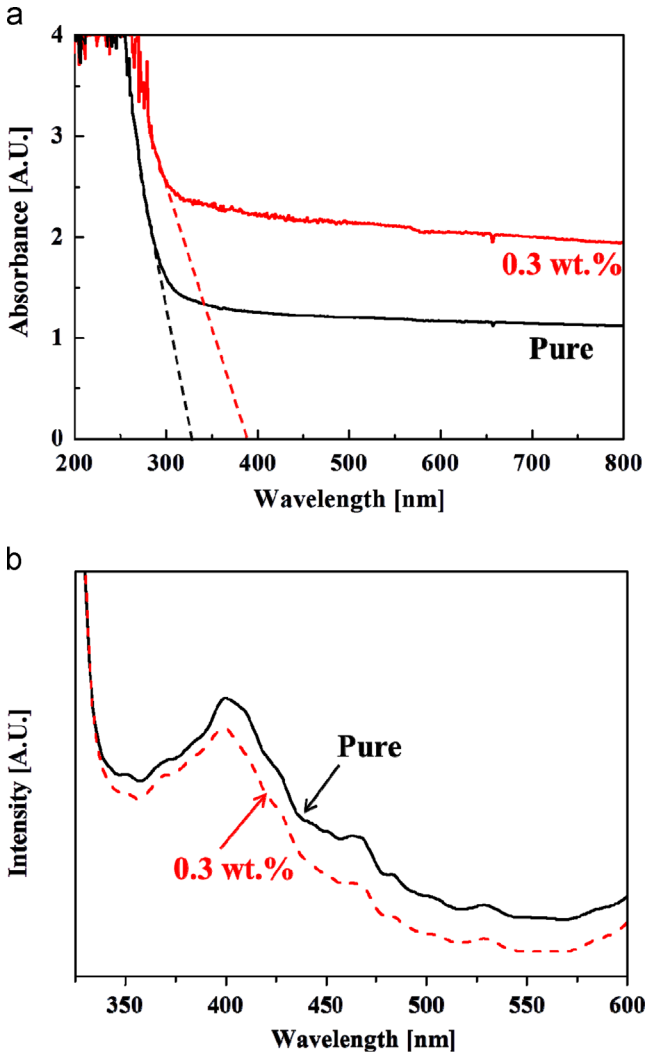

Fig. 8. (a) UV–vis absorbance spectra of the pure and 0.3 wt% and (b) comparison of the photoluminescence spectra of pure and 0.3 wt%.

process [40]. The Ti–C bond prevents charge recombination and enhances the transport of electrons in the G–TiO_2 films as compared to pure TiO_2, consequently increasing the efficiency of the DSSC.

Fig. 8(a) compares the UV–vis absorbance spectra of the pure TiO_2 and 0.3 wt% G–TiO_2 films. The enhanced absorption of the 0.3 wt% G–TiO_2 film in the visible region can be attributed to the presence of graphene, which is thus expected to enhance the efficiency of the DSSC. Furthermore, the noticeable red-shift in the absorption edge of the 0.3 wt% G–TiO_2 film suggests a narrowing of the band gap of TiO_2 due to the presence of graphene as compared with pure TiO_2 [24,41]. The addition of graphene to TiO_2 changes the color of TiO_2 from white to gray.

The photocatalytic activity of the G–TiO_2 films depends on the lifetime of the electron–hole pairs and the trapping of these charges. Photoluminescence (PL) spectroscopy was used to study the efficiency of semiconductor charges, their trapping, migration, and transfer, as well as the recombination of electrons and holes, which emit photons for PL. Fig. 8(b) compares the PL spectra for the pure TiO_2 and 0.3 wt% G–TiO_2 films. Both samples show a similar PL pattern. The peak located at 399 nm is attributed to the emission light with energy almost equal to the band gap energy of anatase (387.5 nm) [42]. The three peaks observed in the wavelength ranging from 440 to 500 nm are attributable to surface oxygen vacancies and defects [43]. The intensity of the PL spectra for the 0.3 wt% G–TiO_2 is low as compared to that of pure TiO_2. This trend clearly indicates that the G–TiO_2 films have a lower recombination rate of electrons and holes under UV-light irradiation. Thus, the addition of graphene to TiO_2 favorably modified the surface properties and reduced the trapping sites, resulting in an enhanced excitation lifetime [44].

The enhanced photocatalytic activity of the G–TiO_2 films under UV illumination is depicted and explained in Fig. 9. When UV light is illuminated on G–TiO_2 via FTO, electrons (e^-) are excited from the valence band (VB) to the conduction band (CB) of TiO_2, leaving a hole (h^+) in the VB. In general, most electrons and holes recombine, and fewer than 1% of the electrons and holes actually participate in photocatalytic

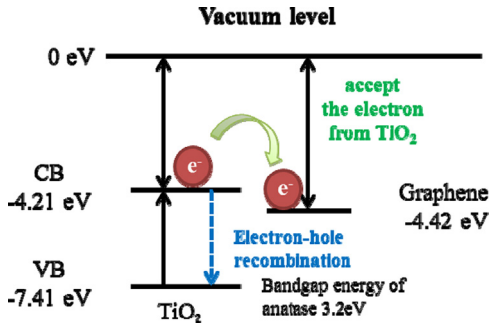

Fig. 9. Schematic diagram of the energy level of TiO_2 and graphene.

reactions, ultimately reducing the photocatalytic efficiency [45,46]. It has been reported that the work function of graphene is −4.42 eV [47] and the CB position of anatase TiO_2 is approximately −4.21 eV with a band gap of approximately 3.2 eV [48], as shown in Fig. 9. The excited electrons from TiO_2 are captured by graphene with minimized obstruction. Thus, graphene interrupts the electron–hole recombination and increases the number of photocatalytic reactions.

4. Conclusions

We synthesized graphene–TiO_2 composites comprising P25 nanopowder and PVA polymer using the supersonic kinetic spraying technique of AD. When these G–TiO_2 films of various graphene concentrations were used as working electrodes in DSSCs, the 0.3 wt% case showed the highest conversion efficiency of 5.02%. XPS, absorbance and photoluminescence spectra explained the optimal performance at 0.3 wt%. A clear trend in conversion efficiency per varying concentrations was observed.

Acknowledgment

This work was supported by the Human Resources Development program (No. 20124030200120) of KETEP. This work was also supported by the Industrial Strategic Technology Development Program (10045221). The authors extend their appreciation to the Deanship of Scientific Research at King Saud University for funding the work through the research group project No. RGP-089.

References

[1] B. O'Regan, M. Grfitzeli, A low-cost, high-efficiency solar cell based on dye-sensitized, Nature 353 (1991) 24.
[2] A. Fujishima, T.N. Rao, D.A. Tryk, Titanium dioxide photocatalysis, J. Photochem. Photobiol. C 1 (1) (2000) 1–21.
[3] Z. Huang, P.C. Maness, D.M. Blake, E.J. Wolfrum, S.L. Smolinski, W.A. Jacoby, Bactericidal mode of titanium dioxide photocatalysis, J. Photochem. Photobiol. A—Chem. 130 (2) (2000) 163–170.
[4] D.M. Blake, P.C. Maness, Z. Huang, E.J. Wolfrum, J. Huang, W.A. Jacoby, Application of the photocatalytic chemistry of titanium dioxide to disinfection and the killing of cancer cells, Sep. Purif. Methods 28 (1) (1999) 1–50.
[5] K. Kabra, R. Chaudhary, R.L. Sawhney, Treatment of hazardous organic and inorganic compounds through aqueous-phase photocatalysis: a review, Ind. Eng. Chem. Res. 43 (24) (2004) 7683–7696.
[6] J. Bisquert, D. Cahen, G. Hodes, S. Rühle, A. Zaban, Physical chemical principles of photovoltaic conversion with nanoparticulate, mesoporous dye-sensitized solar cells, J. Phys. Chem. B 108 (24) (2004) 8106–8118.
[7] S.H. Kang, H.S. Kim, J.-Y. Kim, Y.-E. Sung, Enhanced photocurrent of nitrogen-doped TiO_2 film for dye-sensitized solar cells, Mater. Chem. Phys. 124 (1) (2010) 422–426.
[8] X. Tang, D. Li, Sulfur-doped highly ordered TiO_2 nanotubular arrays with visible light response, J. Phys. Chem. C 112 (14) (2008) 5405–5409.
[9] X. Lü, X. Mou, J. Wu, D. Zhang, L. Zhang, F. Huang, F. Xu, S. Huang, Improved-performance dye-sensitized solar cells using Nb-doped TiO_2 electrodes: efficient electron injection and transfer, Adv. Funct. Mater. 20 (3) (2010) 509–515.
[10] P. Joshi, Y. Xie, M. Ropp, D. Galipeau, S. Bailey, Q. Qiao, Dye-sensitized solar cells based on low cost nanoscale carbon/TiO_2 composite counter electrode, Energy Environ. Sci. 2 (4) (2009) 426–429.
[11] S. Gilje, S. Han, M. Wang, K.L. Wang, R.B. Kaner, A chemical route to graphene for device applications, Nano Lett. 7 (11) (2007) 3394–3398.
[12] T. Cassagneau, J.H. Fendler, High density rechargeable lithium-ion batteries self-assembled from graphite oxide nanoplatelets and polyelectrolytes, Adv. Mater. 10 (11) (1998) 877–881.
[13] W. Hu, C. Peng, W. Luo, M. Lv, X. Li, D. Li, Q. Huang, C. Fan, Graphene-based antibacterial paper, ACS Nano 4 (7) (2010) 4317–4323.
[14] W. Wang, P. Serp, P. Kalck, J.L. Faria, Photocatalytic degradation of phenol on MWNT and titania composite catalysts prepared by a modified sol–gel method, Appl. Catal. B—Environ. 56 (4) (2005) 305–312.
[15] Y. Yu, J.C. Yu, C.-Y. Chan, Y.-K. Che, J.-C. Zhao, L. Ding, W.-K. Ge, P.-K. Wong, Enhancement of adsorption and photocatalytic activity of TiO_2 by using carbon nanotubes for the treatment of azo dye, Appl. Catal. B—Environ. 61 (1) (2005) 1–11.
[16] J. Arana, J. Dona-Rodrıguez, E. Tello Rendón, C. Garriga i Cabo, O. González-Dıaz, J. Herrera-Melián, J. Perez-Pena, G. Colón, J. Navıo, TiO_2 activation by using activated carbon as a support: part I. Surface characterisation and decantability study, Appl. Catal. B—Environ. 44 (2) (2003) 161–172.
[17] Q. Xiang, J. Yu, M. Jaroniec, Enhanced photocatalytic H_2-production activity of graphene-modified titania nanosheets, Nanoscale 3 (9) (2011) 3670–3678.
[18] Y.-B. Tang, C.-S. Lee, J. Xu, Z.-T. Liu, Z.-H. Chen, Z. He, Y.-L. Cao, G. Yuan, H. Song, L. Chen, Incorporation of graphenes in nanostructured TiO_2 films via molecular grafting for dye-sensitized solar cell application, ACS Nano 4 (6) (2010) 3482–3488.
[19] S.R. Kim, M.K. Parvez, M. Chhowalla, UV-reduction of graphene oxide and its application as an interfacial layer to reduce the back-transport reactions in dye-sensitized solar cells, Chem. Phys. Lett. 483 (1) (2009) 124–127.
[20] N. Yang, J. Zhai, D. Wang, Y. Chen, L. Jiang, Two-dimensional graphene bridges enhanced photoinduced charge transport in dye-sensitized solar cells, ACS Nano 4 (2) (2010) 887–894.
[21] O. Akhavan, E. Ghaderi, Photocatalytic reduction of graphene oxide nanosheets on TiO_2 thin film for photoinactivation of bacteria in solar light irradiation, J. Phys. Chem. C 113 (47) (2009) 20214–20220.
[22] Y. Yao, G. Li, S. Ciston, R.M. Lueptow, K.A. Gray, Photoreactive TiO_2/carbon nanotube composites: synthesis and reactivity, Environ. Sci. Technol. 42 (13) (2008) 4952–4957.
[23] K. Zhou, Y. Zhu, X. Yang, X. Jiang, C. Li, Preparation of graphene–TiO_2 composites with enhanced photocatalytic activity, New J. Chem. 35 (2) (2011) 353–359.
[24] H. Zhang, X. Lv, Y. Li, Y. Wang, J. Li, P25-graphene composite as a high performance photocatalyst, ACS Nano 4 (1) (2009) 380–386.
[25] J. Akedo, Aerosol deposition of ceramic thick films at room temperature: densification mechanism of ceramic layers, J. Am. Ceram. Soc. 89 (6) (2006) 1834–1839.
[26] J. Ryu, D.S. Park, B.D. Hahn, J.J. Choi, W.H. Yoon, K.Y. Kim, H.S. Yun, Photocatalytic TiO_2 thin films by aerosol-deposition: from micron-sized particles to nano-grained thin film at room temperature, Appl. Catal. B—Environ. 83 (1–2) (2008) 1–7.
[27] T. Watanabe, S. Fukayama, M. Miyauchi, A. Fujishima, K. Hashimoto, Photocatalytic activity and photo-induced wettability conversion of TiO_2

thin film prepared by sol–gel process on a soda-lime glass, J. Sol–Gel Sci. Technol. 19 (1) (2000) 71–76.
[28] Y.J. Kim, M.H. Lee, H.J. Kim, G. Lim, Y.S. Choi, N.G. Park, K. Kim, W.I. Lee, Formation of highly efficient dye-sensitized solar cells by hierarchical pore generation with nanoporous TiO_2 spheres, Adv. Mater. 21 (36) (2009) 3668–3673.
[29] Y. Ohko, T. Tatsuma, T. Fujii, K. Naoi, C. Niwa, Y. Kubota, A. Fujishima, Multicolour photochromism of TiO_2 films loaded with silver nanoparticles, Nat. Mater. 2 (1) (2002) 29–31.
[30] J.-J. Park, D.Y. Kim, J.G. Lee, D. Kim, J.-H. Oh, T.-Y. Seong, M.F. Hest, S.S. Yoon, Superhydrophilic transparent titania films by supersonic aerosol deposition, J. Am. Ceram. Soc. (2013).
[31] J.J. Park, J.G. Lee, D.Y. Kim, J.H. Hong, J.J. Kim, S. Hong, S.S. Yoon, Antibacterial and water purification activities of self-assembled honeycomb structure of aerosol deposited titania film, Environ. Sci. Technol. 46 (22) (2012) 12510–12518.
[32] S.I. Noh, H.-J. Ahn, D.-H. Riu, Photovoltaic property dependence of dye-sensitized solar cells on sheet resistance of FTO substrate deposited via spray pyrolysis, Ceram. Int. 38 (5) (2012) 3735–3739.
[33] A. Patterson, The Scherrer formula for X-ray particle size determination, Phys. Rev. 56 (10) (1939) 978.
[34] D.Y. Kim, J.J. Park, J.G. Lee, M.W. Lee, H.Y. Kim, J.H. Oh, T.Y. Seong, D. Kim, S.C. James, M.F. Hest, Tuning hydrophobicity with honeycomb surface structure and hydrophilicity with CF_4 plasma etching for aerosol-deposited titania films, J. Am. Ceram. Soc. 95 (12) (2012) 3955–3961.
[35] N. Khalid, E. Ahmed, Z. Hong, Y. Zhang, M. Ahmad, Nitrogen doped TiO_2 nanoparticles decorated on graphene sheets for photocatalysis applications, Curr. Appl. Phys. 12 (6) (2012) 1485–1492.
[36] X.Y. Zhang, H.P. Li, X.L. Cui, Y. Lin, Graphene/TiO_2 nanocomposites: synthesis, characterization and application in hydrogen evolution from water photocatalytic splitting, J. Mater. Chem. 20 (14) (2010) 2801–2806.
[37] N.L. Wu, M.S. Lee, Z.J. Pon, J.Z. Hsu, Effect of calcination atmosphere on TiO_2 photocatalysis in hydrogen production from methanol/water solution, J. Photochem. Photobiol. A—Chem. 163 (1) (2004) 277–280.
[38] E. Serwicka, ESR study on the interaction of water vapour with polycrystalline TiO_2 under illumination, Colloids Surf. 13 (1985) 287–293.
[39] J. Zhang, Z. Xiong, X. Zhao, Graphene–metal–oxide composites for the degradation of dyes under visible light irradiation, J. Mater. Chem. 21 (11) (2011) 3634–3640.
[40] O. Akhavan, R. Azimirad, S. Safa, M. Larijani, Visible light photo-induced antibacterial activity of CNT–doped TiO_2 thin films with various CNT contents, J. Mater. Chem. 20 (35) (2010) 7386–7392.
[41] Y. Zhang, Z.-R. Tang, X. Fu, Y.-J. Xu, TiO_2–graphene nanocomposites for gas-phase photocatalytic degradation of volatile aromatic pollutant: is TiO_2–graphene truly different from other TiO_2–carbon composite materials? ACS Nano 4 (12) (2010) 7303–7314.
[42] J. Yu, T. Ma, S. Liu, Enhanced photocatalytic activity of mesoporous TiO_2 aggregates by embedding carbon nanotubes as electron-transfer channel, Phys. Chem. Chem. Phys. 13 (8) (2011) 3491–3501.
[43] Y. Yu, J.C. Yu, J.-G. Yu, Y.-C. Kwok, Y.-K. Che, J.-C. Zhao, L. Ding, W.-K. Ge, P.-K. Wong, Enhancement of photocatalytic activity of mesoporous TiO_2 by using carbon nanotubes, Appl. Catal. A: Gen. 289 (2) (2005) 186–196.
[44] N. Farhangi, Y. Medina-Gonzalez, R.R. Chowdhury, P.A. Charpentier, Growing TiO_2 nanowires on the surface of graphene sheets in supercritical CO_2: characterization and photoefficiency, Nanotechnology 23 (29) (2012) 294005.
[45] R.I. Bickley, T. Gonzalez-Carreno, J.S. Lees, L. Palmisano, R.J. Tilley, A structural investigation of titanium dioxide photocatalysts, J. Solid State Chem. 92 (1) (1991) 178–190.
[46] G. Li, K.A. Gray, The solid–solid interface: explaining the high and unique photocatalytic reactivity of TiO_2-based nanocomposite materials, Chem. Phys. 339 (1) (2007) 173–187.
[47] R. Czerw, B. Foley, D. Tekleab, A. Rubio, P. Ajayan, D. Carroll, Substrate-interface interactions between carbon nanotubes and the supporting substrate, Phys. Rev. B 66 (3) (2002) 033408.
[48] Y. Xu, M.A. Schoonen, The absolute energy positions of conduction and valence bands of selected semiconducting minerals, Am. Mineral. 85 (3–4) (2000) 543–556.